STAR: Simultaneous Tracking and Recognition through Millimeter Waves and Deep Learning

Prabhu Janakaraj
Department of Computer Science
University of North Carolina at Charlotte
Charlotte, USA
pjanakar@uncc.edu

Kalvik Jakkala
Department of Computer Science
University of North Carolina at Charlotte
Charlotte, USA
kjakkala@uncc.edu

Arupjyoti Bhuyan
Idaho National Laboratory
Idaho Falls, USA
arupjyoti.bhuyan@inl.gov

Zhi Sun
Department of Electrical Engineering
University at Buffalo
Buffalo, USA
zhisun@buffalo.edu

Pu Wang
Department of Computer Science
University of North Carolina at Charlotte
Charlotte, USA
Pu.Wang@uncc.edu

Minwoo Lee
Department of Computer Science
University of North Carolina at Charlotte
Charlotte, USA
Minwoo.Lee@uncc.edu

Abstract—Gait is the human's natural walking style that is a complex biological process unique to each person. This paper aims to exploit millimeter wave (mmWave) to extract fine-grained microdoppler signatures of human movements, which are used as the mmWave gait biometric for user recognition. Towards this goal, a deep microdoppler learning system is proposed, which utilizes deep neural networks to automatically learn and extract the discriminative features in the mmWave gait biometic data to distinguish a large number of people from each other. In particular, our system consists of two subsystems including human target tracking and human target recognition. The tracking subsystem is responsible for detecting the appearance of a human subject, tracking his/her locations and estimating his/her walking velocity. The recognition subsystem utilizes the tracking data to generate the microdoppler signatures as the mmWave biometrics, which are fed into a custom-designed residual deep convolutional neural network (DCNN) for automatic feature extractions. Finally, a softmax classifier utilizes the extracted features for user identification. In a typical indoor environment, a top-1 identification accuracy of 97.45% is achieved for a dataset of 20 people.

Index Terms—Gait Recognition, mmWave Radar, Deep Learning

I. INTRODUCTION

Motivation. Human authentication is an ever challenging problem being addressed for decades. Biometric-based user recognition is once deemed to be a trustable solution for authentication. Most commonly employed biometrics were based on visible light solutions such as retina scan, fingerprint analysis and facial recognition [4]–[6], [11]. Voice recognition solutions are also widely adopted for user authentication. However, all the above mentioned bio-signs require additional efforts from the human subjects to perform authentication. For example, the retina based authentication requires subjects to keep their eyes close to an Iris scanner. Similarly, facial

recognition needs the subject to keep their faces in front of the high resolution multi-dimensional camera to recognize the inherent facial signatures. Fingerprint authentication requires the subject to swipe or keep their finger on a scanner for scanning the ridges and valleys. Moreover, the aforementioned solutions are all based on physiological biometrics, which suffer spoofing attacks where an illegitimate user fools a biometric recognition system by presenting a synthetic forged version of the biometric trait of the genuine user [1]–[3], [7]. To address these limitations, effortless and non-intrusive authentication systems have been investigated by utilizing behavioral biometrics, such as gait and keystroke. In particular, existing study [8] shows that human gait is very hard to spoof or mimic because our own gait works against us when we try to imitate someone elses gait.

Challenges. Initial studies on capturing human gait signatures were still based on visible light sources such as motion capture cameras and 3D Depth sensor based cameras [9]–[11]. These solutions become impractical with significantly degraded performance when there are obstructions and occlusions, lighting conditions are not ideal, or they are deployed in challenging environmental conditions, such as fog and rain. To counter these challenges, radar-based wireless sensing solutions have been exploited to extract gait biometirc features for user identification [19], [20]. However, these solutions can only achieve limited identification accuracy for a small group of people. For example, in [20], 80% accuacy is achieved for 8 human subjects, while 88% accuacy is achieved for 15 human subjects in [19]. The key reasons for the limited performance in existing research are two folds. First, they did not explore the emerging mmWave radar for high-resolution motion detection and capture. Second, they rely on hand-crafted features (such as stride rate) and rudimentary machine learning methods.

Our Solution. In this paper, a deep microdoppler learning system is proposed, which utilizes deep neural networks to

automatically learn and extract the discriminative features in the mmWave gait biometic data to distinguish a large number of people from each other. In particular, our system consists of two subsystems including human target tracking and human target recognition. The tracking subsystem is responsible for detecting the appearance of a human subject, tracking his/her locations and estimating his/her walking velocity. The recognition subsystem utilizes the tracking data to generate the microdoppler signatures as the mmWave biometrics, which are fed into a custom-designed residual deep convolutional neural network (DCNN) for automatic feature extractions. Finally, a softmax classifier utilizes the extracted features for user identification. Moreover, to make sure the system works well in the multipath-rich environments such as indoor scenes, dedicated data-preprocessing solutions, such as high-pass filter, cell averaging constant false alarm rate detector (CA-CFAR), and spectorgram enhancement scheme, are also integrated into the system to mitigate the environment-induced distortions and noise. In a typical indoor environment, a top-1 identification accuracy of 97.45% is achieved for a dataset of 20 people.

The rest of the paper is organized as follows: Section II details the basics, challenges, and system overview of the mmWave biometric identification solution. Section III presents human tracking subsystem, Section IV explains human identification subsystem. Section V presents the experimental results. Section sec:conclusion concludes this paper.

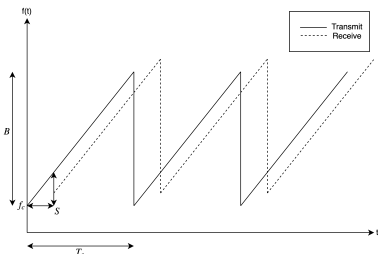## II. SYSTEM DESIGN

A. Preliminaries

Fig. 1: FMCW signal with linear ramp

The fundamental concept in radar systems is the transmission of a signal, which is reflected by the objects in its propagation path. The key advantage of Frequency Modulated Continuous Wave (FMCW) radar system is its capability of measuring the range/location and the velocity of the moving target simultaneously. In particular, the signal used in FMCW radars is called chirp, whose frequency increases linearly with time as shown in Fig. 1. The chirp is characterized by a start frequency (i.e., carrier frequency) f_c, bandwidth B and duration T_c. The slope of the chirp $S = B/T_c$ characterizes the frequency changing rate. The transmitter of the radar sends a chirp signal and the receiver captures the reflected chirp generated by the object. A frequency mixer combines the

transmitted and received chirps to produce the beat signal. For a target at distance d, the beat signal can be described by

$$A \exp(j2\pi(f_0 t + 2d/\lambda_c) = A \exp(j2\pi(2d/\lambda_c)) \exp(j2\pi f_0 t) \tag{1}$$

where A is the signal attenuation gain. $f_0 = 2dS/C$ is called beat frequency. $\lambda_c = C/f_c$ is the wavelength of the carrier frequency where C is the speed of light. Exploiting the beat frequency f_0, the distance of the target can be easily obtained by

$$d = \frac{f_0 C}{2S}. \tag{2}$$

When the target is moving to a new location, the frequency of beat signal will be changed if the distance between the previous location and the new location is larger than the radar range resolution, which is directly related to the bandwidth B, i.e.,

$$d_{res} = \frac{C}{2B}. \tag{3}$$

Due to extremely high carrier frequency of mmwave FMCW radar, very large bandwidth B can be used, which leads to fine-grained range resolution.

While the frequency of the beat signal is used to measure target distance, the phase of the beat signal $\exp(j2\pi(2d/\lambda_c))$ defined in eq. (1) can be exploited to measure the target velocity even if the radar can not detect the location change of the target due to the range resolution constraint. Assume the target moves over an very small distance after N chirps are sent and received, which generates N beat signals. In this case, all N beat signals will have the same beat frequency but with different phases. In particular, the phase of the beat signal $n \in (1, 2, ..., N)$ is equal to

$$\exp(j2\pi(2v/\lambda_c)nT_c) \tag{4}$$

where $2v/\lambda_c$ is called Doppler frequency. The eq. (4) indicates the phases of beat signals for each distinguishable distance constitute a new signal whose carrier frequency is exactly the Doppler frequency. When a human subject is walking, the different human parts (e.g., arms, legs, foots, and torso) move at different velocities, which lead to different Doppler frequencies. The radar can distinguish the movements of two parts only if their speed difference is larger than the velocity resolution, which is determined by the observation duration NT_c and the carrier wavelength λ_c, i.e.,

$$v_{res} = \frac{\lambda_c}{2NT_c}. \tag{5}$$

Since mmWave radar has a wavelength in the scale of millimeters, it characterizes fine-grained motion dynamics of human gait. For example, compared with sub-6GHz radar, the 77GHz mmWave radar can achieve over 12 times higher velocity resolution.

B. mmWave Gait Biometric

The raw mmWave data samples can be collected by using commercial off-the-shelf mmWave radar and these raw samples are converted into mmWave gait biometrics by following

the workflow in Fig. 2. First, the analog beat signal is sampled using the sampling frequency f_s, which leads to the discrete beat signal consisting of $K = T_c f_s$ samples. Then, M beat signals constitute a frame, which can be represented by a $K \times M$ matrix. Next, L frames constitute a observation sample (i.e., mmWave data sample), which consists of $N = ML$ discrete beat signals and can be represented by $K \times N$ matrix. Then, we perform range-FFT on such signal matrix to generate the range-time map. In particular, we perform K-points FFT along each column of the signal matrix to obtain a column of K elements, each of which corresponds to the complex amplitude $A \exp(j2\pi(2d/\lambda_c))$ of a particular beat frequency f_0 defined in eq. (1). If the absolute amplitude for frequency f_0 is non-zero, then based on eq. (2), a target is detected at the range that corresponds to this frequency. Performing range-FFT for all N columns of the signal matrix, we can obtain the range-time map. Then, we apply short-time-Fourier-transform (STFT) over each row (range bin), which leads to K spectrograms. Each spectrogram characterizes the micro-Doppler signatures when the human moves a particular range bin. Next, we combine K spectograms together to generate the mmWave gait biometric.
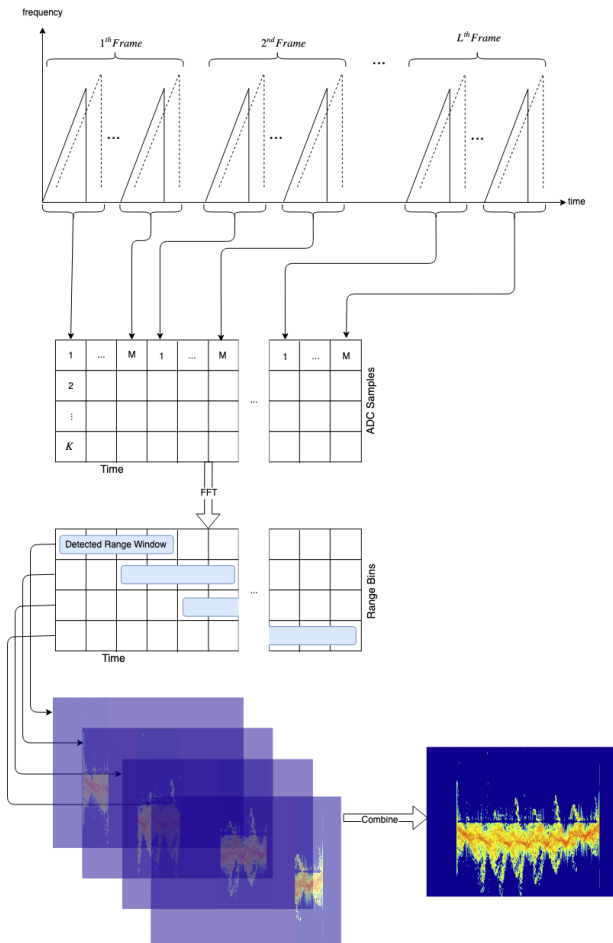

Fig. 2: mmWave Gait Biometric Generation Workflow

C. Challenges

The key challenges to exploit mmWave micro-Doppler signatures for gait recognition are two-fold. First, the micro-Doppler signatures come from the reflections that directly bounce off from human bodies. However, mmWave signals have very short wavelengths and thus can be easily reflected back by surrounding obstructions. These reflections carry the environment-dependent information, which is harmful for the recognition task and has to be removed. In particular, these environment reflections include static ones, which are directly induced by the stationary obstructions (e.g., walls) and dynamics ones, which indirectly bounce from other stationary obstructions and then bounce from human bodies. The harmful environment reflections carry delayed and distorted micro-Doppler information. Second, mmWave gait biometric is of high dimensional data. Therefore, heuristically selecting features from such data is suboptimal, which may fail to characterize the salient and discriminative patterns to distinguish a large number of people from each other. This naturally requires us to implement automatic feature extraction by exploiting deep neural networks.

D. System Overview

Our system consists of two subsystems including human target tracking and human target recognition. The tracking subsystem is responsible for detecting the appearance of a human subject, tracking his/her locations and estimating his/her walking velocity. The traveling locations and traveling time are used to determine the dimension of mmWave data sample (i.e., K and N). The collected data samples from a group of human subjects are then converted into mmWave gait biometric samples, which are fed into the recognition subsystem. The recognition subsystem exploits these samples to train a deep neural network that automatically learns the salient features of the mmWave gait biometrics. The trained network is used to identify the human subjects. To make sure the system works well in the multipath-rich environments (e.g., indoor scenes), dedicated data-preprocessing solutions, such as high-pass filter, cell averaging constant false alarm rate detector (CA-CFAR), and spectorgram enhancement scheme, are also integrated into the system to mitigate the distortions in the mmWave biometric samples caused by environment-induced static/dynamic reflections and background noise. The system architecture is shown in Fig. 3 and the details of each system block are presented in the following sections.

III. HUMAN TARGET TRACKING

A. Range-Doppler Map with Static Reflection Suppression

The target tracking is based on the range-Doppler map, which is generated by performing 2D-FFT on each mmWave data frame, i.e., first performing FFT across each column (range-FFT) to create range-time matrix and then applying FFT across each range bin (Doppler-FFT) of range-time map to generate range-Dopper map. The peaks in the cells of the range-Dopper map represent the detected targets associated with their radical velocities and locations relative to the
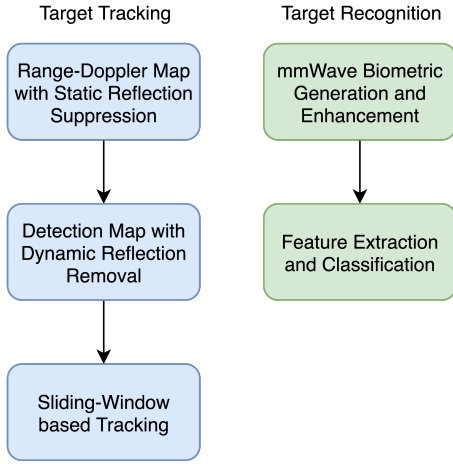
Range-Doppler Map
with Static Reflection
Suppression

mmWave Biometric
Generation and
Enhancement

Detection Map with
Dynamic Reflection
Removal

Feature Extraction
and Classification

Sliding-Window
based Tracking

Fig. 3: System Overview

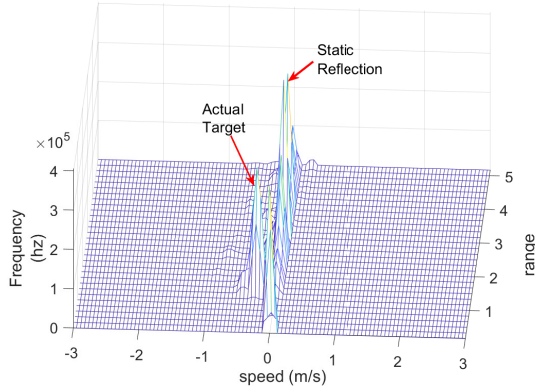Fig. 5: Highpass-filtered Range-Doppler Map with Dynamic Reflections

Fig. 4: Range-Doppler Map with Static Reflections

radar. However, as shown in Fig. 4, the static objects in the background environment such as chairs, tables, can induce the static reflections that generate undesired peaks along the zero velocity line. To remove these static reflections, we apply an 8th-order butterworth high-pass filter with cutoff frequency of 100Hz on each row of range-time map and then apply Doppler-FFT on the filtered range-time map.

B. Detection Map with Dynamic Reflection Removal

Using the range-Doppler map, the target detection map can be generated, which labels the detected moving targets as 1s in the corresponding cells of the range-Doppler map. Towards this goal, we first need to remove dynamic environment reflections, which can generate multiple fake targets as shown in Fig. 5. The dynamic reflections come from the signals that bounce from walls and then bounce from human subjects. Thus, those signals travel over long propagation paths to arrive at the radar receiver. Therefore, their energy levels are generally lower, compared with the signals directly reflected from the human subjects. Therefore, by treating the dynamic reflections as noise, we can adopt CA-CFAR [25], which is one of most commonly used target detectors in radar theory
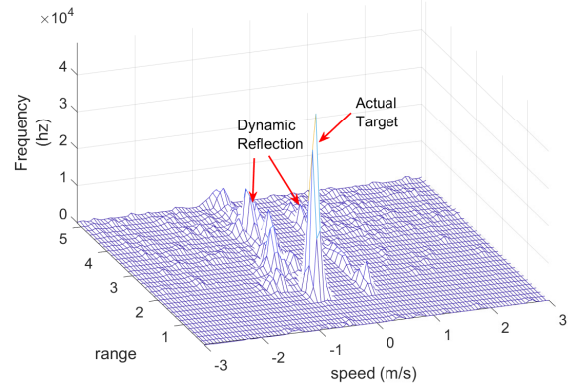
for noisy and interference-rich environments. The key idea of CA-CFAR is to determine whether a target is present or not by comparing its energy to an adaptive threshold T. The threshold is a function of the desired false-alarm probability and the estimated noise level that is computed by taking the mean of neighbouring cells around the cell-under-test. However, the key challenge to directly apply CA-CFAR for human subject detection is that different parts (e.g., torso and legs) of a human move at different velocities so that the bulk motion of torso generates the main Doppler component that is modulated by the micro-Doppler components from the swinging arms and legs. This can create a cluster of closely-located peaks with comparable energy levels in the range-Doppler map. Such phenomenon can significantly affect the detection performance of CA-CFAR. To address this challenge, before applying CA-CFAR, we exploit the percentile method in [25] to only localize the cells in the range-Doppler map which correspond to torso reflections. Using the threshold from CA-CFAR, the cells with torso reflections can be labelled as 1's and other cells are labeled as 0's. Then, the cells with 1's are merged a single connected component. The connected component is replaced as a single point by its centroid, which generates the final binary detection map as shown in Fig. 6.
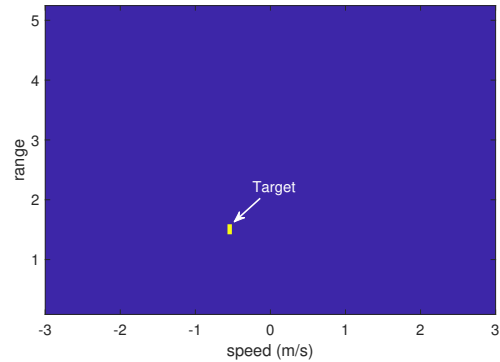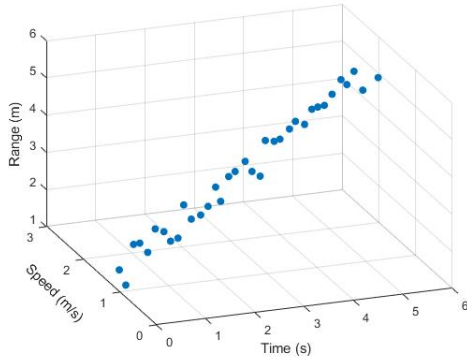

Fig. 6: Detection Map

Fig. 7: Range-Velocity-Time Map for Human Tracking

C. Sliding-Window based Tracking

Based on the detection map, we first identify the target presence by checking whether a peak with non-zero velocity appear or not. Once a target is identified, we initiate the tracking by locking the target's location within the range-Doppler map. Then, a detection map is generated for every radar data frame. Since the target's approximate velocity is also available from the detection map, a 2D window is employed to continuously track the position of the target as shown in Fig. 7 tracking. By moving the window across the detection maps, we can keep tracking the target at various time instances. In particular, this window predicts the potential area the target will move to during next data frame. The length of the moving window estimates the predicted moving distance of the human between two radar frames and is set to be $2vT_f$, where v is the estimated velocity and T_f is time duration of the radar frame that is equal to the number of chirps per-frame M times the chirp duration T_c. The width of the window is determined according to the velocity variance. In our case, we set it to be $0.5 m/s$. Figure 7 shows a walking trace of a tracked human subject, which shows walking range and velocity at each time instance.

IV. HUMAN TARGET IDENTIFICATION - DEEP MICRO-DOPPLER LEARNING

A. mmWave Biometric Generation and Enhancement

The tracking subsystem can tell the walking range and time information, which is used to extract the mmWave raw data that contains the human movements. Then, we apply range-FFT on the extracted mmWave data to generate the range-time map. The range-time map, as shown in Fig. 8a, is pre-processed to remove static and dynamic environment reflections. Similar to the tracking subsystem, the static reflection removal is adopted on the range-time map by applying butterworth high-pass filter for each range bin. Then, dynamic reflection removal is initiated. In particular, we apply CA-CFAR and windowing technique, similar to the ones used for tracking, in each range bin to extract the samples that contains human movements, while zeroing-out the harmful dynamic reflections. The pre-processed range-time map in
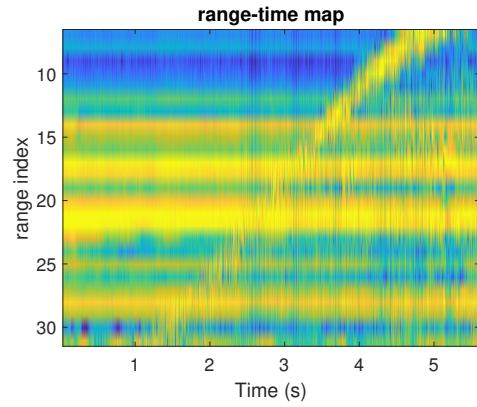
(a) Range-Time Map
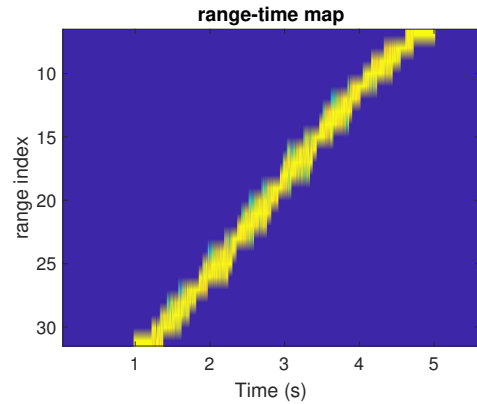
(b) Pre-processed Range-Time Map

Fig. 8: (a) Range-Time Map (b) Pre-processed Range-Time Map

Fig. 8b is converted into a mmWave biometric sample, which is an aggregated spectrogram as demonstrated in Section II.B. To improve recognition accuracy, we further enhance the spectrogram. First, the spectrogram is normalized by dividing the amplitude of each point in the spectrogram with the total energy of the spectrogram, which is the sum of the amplitudes of all points in the spectrogram. Second, mean filtering is applied by calculating the mean of the spectrogram, which is treated as the estimated noise floor. Then, the noise floor is subtracted from the spectrogram. Third, a 2D-Gaussian filter is convolved over the spectrogram to further reduce noise. The enhanced mmWave gait biometric is shown in figure 9.

B. Feature Extraction and Classification

We use a DCNN to learn high-level salient features from mmWave biometric data samples. We found that Residual DC-NNs (ResNets) [22], which are DCNNs with residual layers, outperform most of the currently popular DCNN architectures for mmWave biometric recognition. Residual layers are stacks of convolutional, activation, batch normalization and addition layers with a skip connection. The skip connection allows the features to propagate forward via both the main stack of layers and the skip connection bypassing the primary stack. This promotes better feature extraction and gradient
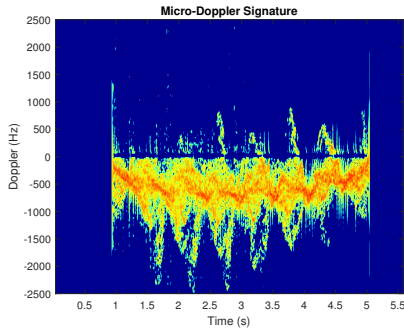
Fig. 9: mmWave gait biometric with torso carrying high-energy low-frequency microdoppler signatures (darker color) and arms/foots inducing low-energy high-frequency microdoppler signatures

layer	output size	layer parameters		
conv1	64×512	7×7, 32, stride 2		
maxpool1	32×256	3×3, stride 2		
conv2_x	16×128	$1 \times 1,$ 32 $3 \times 3,$ 32 $1 \times 1,$ 128	$\times 2$	
conv3_x	8×64	$1 \times 1,$ 64 $3 \times 3,$ 64 $1 \times 1,$ 256	$\times 2$	
conv4_x	4×32	$1 \times 1,$ 64 $3 \times 3,$ 64 $1 \times 1,$ 256	$\times 2$	
bottleneck	1×1	average pool, 20-d fc, softmax		

TABLE I: Parametric overview of Resnet

Parameter	Value
Frequency	77G
Bandwidth	900.9Mhz
Ramp Slope	15Mhz
ADC Samples	256
Sampling rate	5Msps
No.of.Frames	200
No.of Chirps	230
Periodicity	33.00

TABLE II: Texas Instruments IWR1642 mmWave device parameters

flow during back propagation. In particular, we construct a custom-designed 14-layer ResNet following the architectural design principles as defined in [22]. We utilize 2 types of residual layers, identity and convolutional residual layers. The identity residual layers do not have any operations on the skip connection and maintain the feature map's height and width. The convolutional residual layers have convolutional and batch normalization operations in the skip connections, and the operation reduces the dimension of the output feature map. The detailed network structure is illustrated in Fig. 10 and its parameters are listed in Table I. The high level features extracted by the ResNet are passed on to a softmax classifier which converts the features to class likelihoods:

$$y_{ic} = P(c|i) = \frac{\exp^{Z(c)}}{\sum_{j=1}^{C} \exp^{Z(j)}}. \tag{6}$$

The class with the maximum likelihood is considered as the classifier's prediction:

$$c^* = argmax_{c \in C} P(c|i). \tag{7}$$

The model's predictions along with the true labels are used to compute cross entropy loss for backpropagtion to upate the model's weights [23]:

$$L(t, y) = -\sum_{i=1}^{N} \sum_{c \leq C} t_{ic} log(y_{ic}). \tag{8}$$

V. EXPERIMENTAL VALIDATION

A. Experimental Setup

Our mmWave FMCW radar system (Fig. 11) is from Texas Instruments (TI) IWR1642EVM boost board interfaced with a DCA1000EVM board to capture the raw radar samples, which are processed using the custom-designed system blocks proposed in this paper. Our radar system has 2 transmitting antennas, 4 receiving antennas, and $120°$ field of view of azimuth plane. The radar system operates from 77 Ghz to 81 Ghz covering upto a 4 Ghz bandwidth. A Dell Latitude 7480 laptop with TI mmWave studio software is used as a

control system for our radar device to configure the FMCW wave parameters such as chirp width, repetition time and chirp slope. Table II lists the key parameters that we used for our data collection.

.

B. Dataset Construction and Training Methodology

We recruited 20 volunteers to create our dataset. Each participant was asked to walk in his/her natural way in a office area shown in Fig. 11. A participant can either walk towards the radar or walk away from the radar, each of which is counted as one walking instance. We asked each participant to finish 90 walk instances that lead to 90 raw radar samples per participant. Each raw radar sample is then converted to a mmWave gait biometric sample by following the procedures proposed in the previous section. Each biometric sample has a dimension of 128×1024. The dataset was split into training and testing set by randomly selecting samples for each set. We used a 85-15 train-test split ratio and a 10 fold Monte Carlo cross validation was performed, with a mini batch size of 32. The Adam optimizer [23] was used to train the model with an initial learning rate of 1×10^{-4} and a decay rate of 1×10^{-3} for 250 epochs.

C. User Identification Accuracy

DCNNs are trained on the training set, and the test set is used to monitor the model's performance on unseen data. The testing set is not used to update the weights of the DCNN which allows us to quantify the model's real world performance. The train and test accuracies are defined as follows:

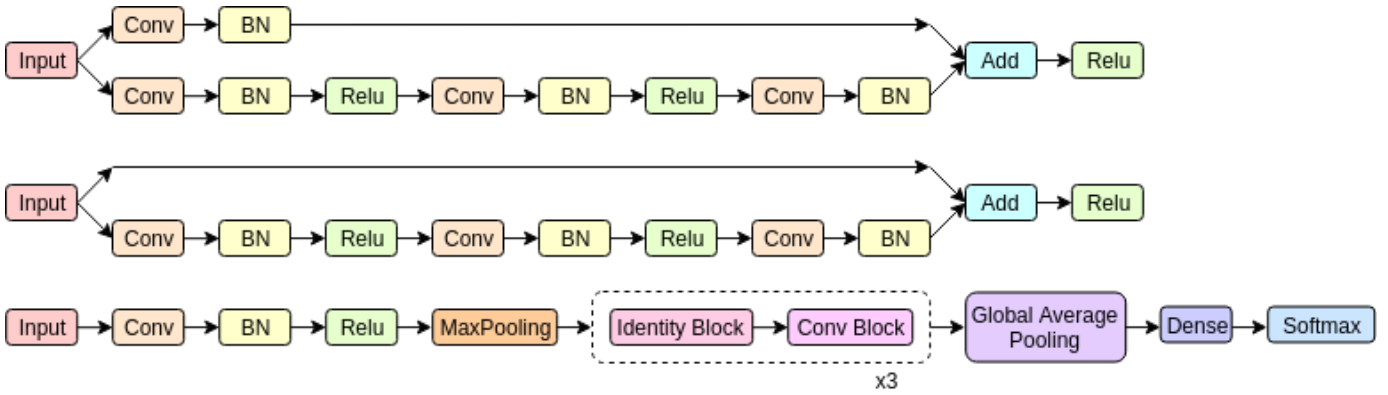$$Train\ Accuracy = \frac{\text{# of correct predictions from train set}}{\text{# of samples in train set}},$$

Fig. 10: (Top) Convolutional Residual layer, (Middle) Identity Residual layer,(Bottom) Resnet Architect Overview
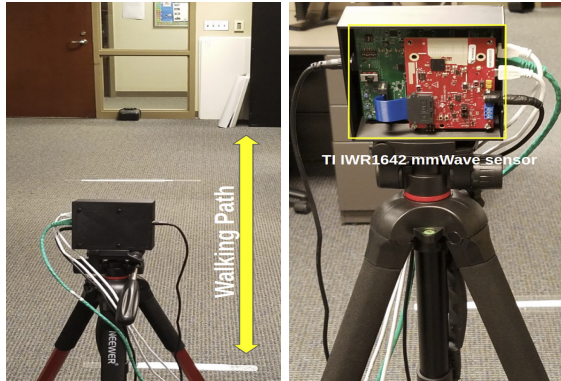

Fig. 11: (Left) Data collection environment. (Right) TI mmWave device

$$Test\ Accuracy = \frac{\#\ of\ correct\ predictions\ from\ test\ set}{\#\ of\ samples\ in\ test\ set}.$$

Our approach achieves a mean testing accuracy of $97.45 \pm 1.13\%$. Fig. 12 shows the convergence of the model test accuracy over 10-fold cross validation.
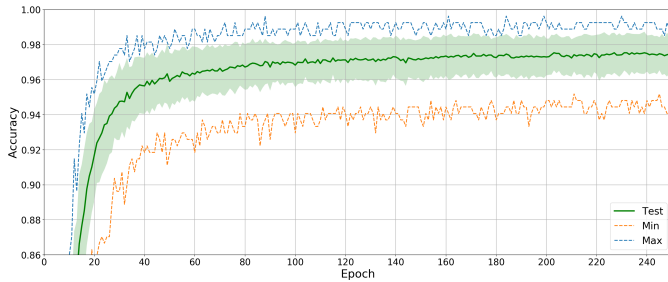

Fig. 12: Test accuracy of 10-fold Monte Carlo cross validation.

D. Confusion Matrix

The confusion matrix is utilized to show model performance over each class in the dataset. A confusion matrix has 4 metrics true positive (TP), true negative (TN), false positive (FP) and false negative (FN). The four metrics define different ratios of negative and positive samples, where positive samples are the samples which belong to the class of interest and

negative samples are defined as the samples which don't belong to the class of interest. The confusion matrix for a model trained on our dataset is shown in Fig. 13. The diagonal elements of the matrix describe the TPs for each class. After deleting the diagonal elements, the remaining elements of each row represent the FPs and the remaining elements of each column characterize the FNs. It is shown that our system can consistently achieve high true positive rate (low true negative rate) along with low false positive and false negative rates for all classes/human subjects.
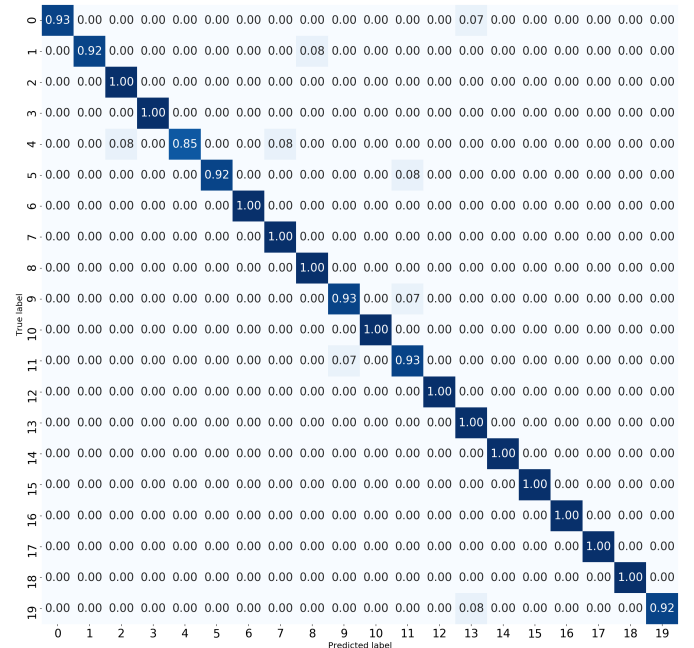

Fig. 13: Confusion matrix for a model trained on our dataset

E. Classification Report

We also present the classification report for our system. The report consists of 3 metrics: precision, recall and F1-score which are computed from the four metrics (TP, TN, FP and FN) used in confusion matrix. The three metrics are defined below. The precision score is the confidence of the classifier

to identify samples of a class, recall defines the classifier's ability to identify all relevant cases in the dataset. The F1-score is interpreted as the weighted average of precision and recall. The classification report is shown in Fig. 14. We can observe that our system achieve achieve very high (over 95%) precision, recall and F1 scores for almost every human subject.

$$Precision = \frac{TP}{(TP + FP)},$$
$$Recall = \frac{TP}{TP + FN},$$
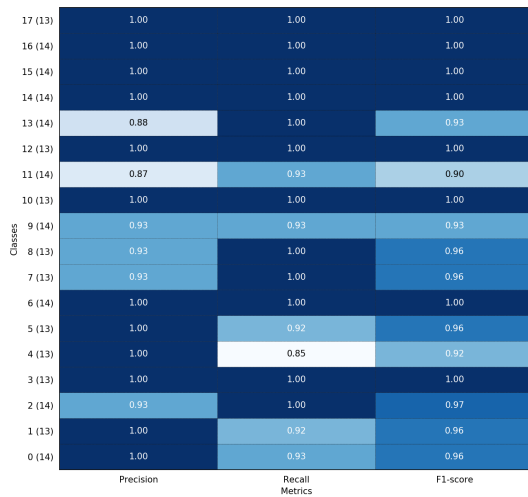$$F1 = \frac{2(Recall \times Precision)}{(Recall + Precision)}.$$

Fig. 14: Average test accuracy of 8, 18-layer ResNets. Each network is trained on a randomly selected train and test set.

VI. CONCLUSION

This paper proposed a deep learning system for user recognition based on mmWave gait biometrics. Two subsystems, human target tracking and human target identification, are implemented first to track user's locations and estimate user's walking velocity and next to identify/classify users. We produce the high-resolution microdoppler signatures as the mmWave biometrics, which are successfully used for human identification in the second subsystem. A custom-design, ResNet learns the salient features embedded in the high-dimensional mmWave biometric samples. For training and testing, we collected 20 different gait patterns from volunteers and achieved 97.45% of classification accuracy.

REFERENCES

[1] N. Kose and J. Dugelay, "On the vulnerability of face recognition systems to spoofing mask attacks," 2013 IEEE International Conference on Acoustics, Speech and Signal Processing, Vancouver, BC, 2013, pp. 2357-2361.
[2] R. Raghavendra, K. B. Raja, S. Venkatesh, F. A. Cheikh and C. Busch, "On the vulnerability of extended Multispectral face recognition systems towards presentation attacks," 2017 IEEE International Conference on Identity, Security and Behavior Analysis (ISBA), New Delhi, 2017, pp. 1-8.
[3] N. Erdogmus and S. Marcel, "Spoofing Face Recognition With 3D Masks," in IEEE Transactions on Information Forensics and Security, vol. 9, no. 7, pp. 1084-1097, July 2014.
[4] J. Galbally, S. Marcel and J. Fierrez, "Biometric Antispoofing Methods: A Survey in Face Recognition," in IEEE Access, vol. 2, pp. 1530-1552, 2014.
[5] C. Raghavendra, A. Kumaravel and S. Sivasubramanian, "Iris technology: A review on iris based biometric systems for unique human identification," 2017 International Conference on Algorithms, Methodology, Models and Applications in Emerging Technologies (ICAMMAET), Chennai, 2017, pp. 1-6.
[6] Yang, W.; Wang, S.; Hu, J.; Zheng, G.; Valli, C. Security and Accuracy of Fingerprint-Based Biometrics: A Review. Symmetry 2019, 11, 141.
[7] A. Hadid, N. Evans, S. Marcel and J. Fierrez, "Biometrics Systems Under Spoofing Attack: An evaluation methodology and lessons learned," in IEEE Signal Processing Magazine, vol. 32, no. 5, pp. 20-30, Sept. 2015
[8] S. Wang, J. Zhang, and L. Tong, Walk the walk: Attacking gait biometrics by imitation, in Proc. International Conference on Information Security, 2010, pp. 361 380.
[9] Ju Han and Bir Bhanu, "Individual recognition using gait energy image," in IEEE Transactions on Pattern Analysis and Machine Intelligence, vol. 28, no. 2, pp. 316-322, Feb. 2006.
[10] J. Lu, G. Wang and P. Moulin, "Human Identity and Gender Recognition From Gait Sequences With Arbitrary Walking Directions," in IEEE Transactions on Information Forensics and Security, vol. 9, no. 1, pp. 51-61, Jan. 2014.
[11] M. Gabel, R. Gilad-Bachrach, E. Renshaw and A. Schuster, "Full body gait analysis with Kinect," 2012 Annual International Conference of the IEEE Engineering in Medicine and Biology Society, San Diego, CA, 2012, pp. 1964-1967.
[12] A. Pokkunuru, K. Jakkala, A. Bhuyan, P. Wang and Z. Sun, "NeuralWave: Gait-Based User Identification Through Commodity WiFi and Deep Learning," IECON 2018 - 44th Annual Conference of the IEEE Industrial Electronics Society, Washington, DC, 2018, pp. 758-765
[13] W. He, K. Wu, Y. Zou and Z. Ming, "WiG: WiFi-Based Gesture Recognition System," 2015 24th International Conference on Computer Communication and Networks (ICCCN), Las Vegas, NV, 2015, pp. 1-7.
[14] Z. Wang, B. Guo, Z. Yu and X. Zhou, "Wi-Fi CSI-Based Behavior Recognition: From Signals and Actions to Activities," in IEEE Communications Magazine, vol. 56, no. 5, pp. 109-115, May 2018.
[15] Yeonghwan Ju, Youngseok Jin and Jonghun Lee, "Design and implementation of a 24 GHz FMCW radar system for automotive applications," 2014 International Radar Conference, Lille, 2014, pp. 1-4.
[16] A. Shoykhetbrod, A. Hommes and N. Pohl, "A scanning FMCW-radar system for the detection of fast moving objects," 2014 International Radar Conference, Lille, 2014, pp. 1-5.
[17] Y. Kim and H. Ling, "Human Activity Classification Based on Micro-Doppler Signatures Using a Support Vector Machine," in IEEE Transactions on Geoscience and Remote Sensing, vol. 47, no. 5, pp. 1328-1337, May 2009.
[18] Y. Kim and T. Moon, "Human Detection and Activity Classification Based on Micro-Doppler Signatures Using Deep Convolutional Neural Networks," in IEEE Geoscience and Remote Sensing Letters, vol. 13, no. 1, pp. 8-12, Jan. 2016.
[19] Fadel Adib, Chen-Yu Hsu, Hongzi Mao, Dina Katabi, and Frdo Durand. 2015a. Capturing the human figure through a wall. ACM Transactions on Graphics 34, 6 (2015)
[20] Dave Tahmoush and Jerry Silvious. 2009. Radar micro-doppler for long range front-view gait recognition. In Proc. IEEE BTAS
[21] Mark Richards, Fundamentals of Radar Signal Processing, McGraw Hill, 2005
[22] He, Kaiming, et al. "Deep residual learning for image recognition." Proceedings of the IEEE conference on computer vision and pattern recognition. 2016.
[23] Goodfellow, Ian, Yoshua Bengio, and Aaron Courville. Deep learning. MIT press, 2016.
[24] M. Richards, Fundamentals of Radar Signal Processing. McGraw-Hill, 2005.
[25] P Van Dorp and FCA Groen. Feature-based human motion parameter estimation with radar. IET Radar, Sonar Navigation 2(2) (2008), 135145.